1350 *Chem. Mater.* **2010,** *22,* 1350–1366
DOI:10.1021/cm901969c

CHEMISTRY OF MATERIALS
Article

Annealing Effect on the Magnetic Properties of Polyol-made Ni−Zn Ferrite Nanoparticles

Z. Beji,[†,‡] L. S. Smiri,[‡] N. Yaacoub,[§] J.-M. Grenèche,[§] N. Menguy,[∥] S. Ammar,*[,†] and F. Fiévet[†]

[†]*ITODYS, Université Paris 7, UMR-CNRS 7086, 15 Rue Jean de Baïf 75205 Paris, France,* [‡]*LSSMI, Département de Chimie, Faculté des Sciences de Bizerte, 7021 Zarzouna, Tunisia,* [§]*LPEC, Université du Maine, UMR-CNRS 6087, Avenue Messiaen 72085 Le Mans, France, and* [∥]*IMPMC, Université Paris 6, Université Paris 7, UMR-7590 CNRS, 140 Rue Lourmel 75015 Paris, France*

Received July 2, 2009. Revised Manuscript Received October 27, 2009

The effects of annealing on the magnetic properties of nanocrystalline $Ni_{1-x}Zn_xFe_2O_4$ ($x = 0.2$, 0.4) have been studied. The as-prepared $x = 0.2$ and 0.4 samples with the particle size of about 6 nm present a relatively low blocking temperature of about 47 and 53 K, respectively, as derived from the peak of the zero-field-cooled direct current (dc) susceptibility measurements. The particle size significantly increases after annealing. Up to the annealing temperature of 800 °C, the blocking temperature is found to increase with increasing particle size, whereas the effective anisotropy constant exhibits a maximum for an annealing temperature of 400 °C. The latter effect is attributed to two antagonist contributions: the first one is related to the partial densification of the particles which introduces canting in the crystal interfaces while the second one is related to the size increase of the particles which reduces the surface anisotropy contribution.

Introduction

Nanosized magnetic materials in general and soft Ni−Zn ferrite ones in particular have many attractive properties and there are compelling technical interests in using them in a wide variety of commercial applications ranging from high-density magnetic recording to energy devices such as in inductors and dc−dc (direct current) power converters or cores capable of working at higher frequencies. When the size of the magnetic particle is smaller than the critical size for multidomain formation, the particle exists in a single-domain state while the domain−wall resonance is avoided, favoring thus optimal working conditions at high frequencies. The critical radius, R_c, below which magnetic particles are described as single domains, is approximately $A^{1/2}/M_s$ where A is the exchange constant and M_s the magnetic moment per unit volume.[1] The critical R_c value is estimated to be about 22.3 nm for isolated Ni−Zn ferrite nanoparticles and about 727 nm for those close-packed in a soft environment.[2] A second critical size R'_c, lower than R_c, exists below which the particles suffer from the presence of the magnetic relaxation process resulting from the thermal effect and the existence of energy barriers ΔE separating the local minima of the different equilibrium states of the system. ΔE is directly related to the particle size and the effective anisotropy energy constant.[3] As a result, the magnetization of the particles becomes blocked below the blocking temperature T_B for which the experimental time window is equal to the relaxation time τ characteristic of the particles. For an assembly of noninteracting particles, the relaxation time is generally assumed to be given by the Néel−Brown expression.[4] The main consequence is that for particles with a diameter smaller than $2R'_c$ T_B is largely lower than room temperature, which is a drawback of many of the previously cited applications. The particles become superparamagnetic with a zero coercivity at the temperature of operation.[5] The R'_c value was experimentally estimated to be less than 10 nm for noninteracting Ni−Zn ferrite nanoparticles.[6] Increasing the particle size up to the critical R'_c value, and below R_c, permits one to overcome this drawback and still to benefit from the magnetic single-domain specificities.

Usually fine Ni−Zn ferrite nanoparticles are produced by soft chemical routes involving micellar route, sol−gel, aqueous coprecipitation, and polyol processes. The average diameter of the as-prepared nanoparticles is generally found to be some nanometers lower than the $2R'_c$ limit. Subsequent annealing treatments are then required to tune the crystalline particle growth. Nevertheless, a close inspection of the relevant literature shows that among the magnetic properties affected by the heating process, the

*Corresponding author. E-mail: ammarmer@univ-paris-diderot.fr. Mailing address: Université Paris Diderot, Bâtiment Lavoisier, 15 Rue Jean de Baïf 75205 Paris, France. Phone: (33)1 57 27 87 62. Fax: (33)1 57 27 72 63.

(1) Frei, E. H.; Shtrikman, S.; Treves, D. *Phys. Rev.* **1957**, *106*, 446.
(2) Aharoni, A.; Jakubovics, J.-P. *J. Phys. IV France* **1998**, *8*, 389.
(3) Stoner, E. C.; Wohlfarth, E. P. *Philos. Trans. R. Soc. A* **1948**, *240*, 599.
(4) (a) Néel, L. *Ann. Geophys.* **1949**, *5*, 99. (b) Brown, W. F. *Phys. Rev. B* **1963**, *130*, 1677.
(5) Leslie-Pelecky, D. L. *Chem. Mater.* **1996**, *8*, 1770.
(6) Fang, J.; Shama, N.; Tung, L.-D.; Shin, E. Y.; O'Connor, C. J.; Stokes, K. L.; Caruntu, G.; Wiley, J. B.; Spinu, L.; Tang, J. *J. Appl. Phys.* **2003**, *93*, 7483.

Published on Web 01/07/2010

saturation magnetization, M_{sat}, and the coercivity, H_c, measured in the blocked state are markedly annealing temperature dependent, and their dependency with the annealing temperature is rather more complex than a simple particle size increase effect.

Generally, M_{sat} increases with the heating temperature due to the crystallinity improvement and also to the particle size increase. This is particularly true for Ni−Zn ferrite nanoparticles prepared by chemical routes.[7,8] The particle size increase leads to a reduction in atomic surface-to-volume ratio, reducing the surface effects. Indeed, the finite size of the particles and consequently the break of the magnetic paths at the surface create a magnetic dead layer. The values of saturation magnetization in most of the as-prepared particles are lower than those characteristic of their bulk counterparts. They tend to the bulk values for sufficiently high heating temperature (usually higher than 800 °C).[9] However, some exceptions have to be noticed: for nanocrystalline Ni−Zn ferrite powders, Suawalka et al. for instance reported a decrease of the saturation magnetization with a heating temperature increasing and supposed that a cation distribution change might take place under heating affecting thus the magnetic properties of these materials.[10]

The dependence of the coercivity, measured in the blocked state of the particles, on heating temperature was also explored. It was found out that the coercivity of the particles initially increased with heating temperature (namely with size)[9] up to a threshold value and started to degrade with further size increment.[11] The maximum coercivity of the magnetic particle is usually observed in the single domain region.[7] But, some authors claimed that the maximum of H_c corresponds to the transition from the single domain to the multidomain regime.[12] In addition, a minimum of coercivity was observed in nanocrystalline $Ni_{1-x}Zn_xFe_2O_4$ ($x \leq 0.5$) films annealed 400 °C.[13] This minimum was assumed to be due to a structural change from the as-prepared materials to the annealed one at 400 °C. The authors supposed that the particular synthesis conditions of the films (sputtering on nonheated fused quartz and Si(100) substrate) favor a large proportion of Ni^{2+} cations located in the tetrahedral sites of the spinel structure leading to an increase in the magnetocrystalline anisotropy and a drop in the magnetic moment. The tetrahedrally coordinated Ni^{2+} ions exhibit a strong spin−orbital coupling compared to the octahedral coordinated ones (the fundamental spectroscopic term of tetrahedrally coordinated Ni^{2+} is $^3T_2$ while it is $^3A_{2g}$ for the octahedrally coordinated one). When the films are annealed, the cation distribution tends to that observed in the bulk, giving rise to a drop in anisotropy and, hence, in coercivity. Except for this anomaly, increasing the annealing temperature induces a grain size increase coupled to a coercivity increase. On the contrary, for nonannealed ultrafine ferrite particles, such $CoFe_2O_4$ particles, prepared directly by a chemical route, namely the polyol process, with different average diameters, we observed an increase of the coercivity when the particle size decreases, down to a certain limit. This behavior is mainly due to the enhancement of the surface anisotropy with size reduction.[14]

It appears clearly that the analysis of the heating effect as a merely particle size increase effect is not sufficient. Obviously, heating improves the crystalline state enhancing the saturation magnetization and induces partial densification affecting the strength of dipolar interactions. Moreover, large polycrystalline particles could be formed when the annealing temperature was sufficiently increased. Within a polycrystalline particle, the exchange coupling between nanoparticles with different crystal orientations tends to average the magnetocrystalline anisotropy involving a decrease of the effective anisotropy of the particle assembly. Heating allows also atomic diffusion into each particle or from one particle to another one modulating thus their chemical homogeneity and/or their local structure acting directly on their magnetic properties. In all the previously cited work, these effects are seldom considered. The annealing effect must be analyzed as a complex effect with potential chemical, structural, and microstructural impacts on the magnetic behavior of soft ferrite particles in particular and granular magnetic nanomaterials in general.

For all these reasons, we systematically investigated the effect of annealing at different temperatures on the magnetic properties of $Ni_{1-x}Zn_xFe_2O_4$ ($x < 0.5$) ferrite nanoparticles, focusing on the evolution of both their structural and microstructural properties with heating. We voluntary chose to work on weakly Zn-substituted ferrite to avoid Yafet−Kittel canting emergence. The values $x = 0.2$ and 0.4 were chosen in order to have representative samples of the $Ni_{1-x}Fe_xO_4$ solid solution within the composition range for which the magnetic ordering is a collinear Néel-like ferrimagnetism. These model particles were produced by the polyol process,

(7) Chiu, W. S.; Radiman, S.; Abd-Shukor, R.; Abdullah, M. H.; Khiew, P. S. *J. Alloy. Compds.* **2008**, *459*, 291.
(8) (a) Hessien, M. M.; Rashad, M. M.; El-Barawy, K.; Ibrahim, I. A. *J. Magn. Magn. Mater.* **2008**, *320*, 1615. (b) Nakashima, S.; Fujita, K.; Tanaka, K.; Hirao, K.; Yamamoto, T.; Tanaka, I. *J. Magn. Magn. Mater.* **2007**, *310*, 2543. (c) Yan, S.; Yin, J.; Zhou, E. *J. Alloy. Compds.* **2008**, *450*, 417.
(9) Rao, B. P.; Kim, C.-O.; Kim, C.-G.; Dumitru, I.; Spinu, L.; Caltun, O. F. *IEEE Trans. Magn.* **2006**, *42*, 2858.
(10) Suwalka, O.; Sharma, R. K.; Sebastian, V.; Lakshmi, N.; Venugopalan, K. *J. Magn. Magn. Mater.* **2007**, *313*, 198.
(11) Rajendran, M.; Pullar, R. C.; Bahattacharya, A. K.; Das, D.; Chintalapudi, S. N.; Majumdar, C. K. *J. Magn. Magn. Mater.* **2001**, *232*, 71.
(12) Chinnasamy, C. N.; Jeyadevan, B.; Shinoda, K.; Tohji, K.; Djayaprawira, D. J.; Takahashi, M.; Joseyphus, R. J.; Narayanasamy, A. *Appl. Phys. Lett.* **2003**, *83*, 2862.
(13) Dessai, M.; Prasad, S.; Venkataramani, N.; Samajdar, I.; Nigam, A. K.; Keller, N.; Krishnan, R.; Baggio-Saitovitch, E. M.; Pujada, B. R.; Rossi, A. *J. Appl. Phys.* **2002**, *91*, 7592.
(14) Artus, M.; Ammar, S.; Herbst, F.; L. Ben Tahar, Smiri, L.; Villain, F.; J.-M. Grenèche F. Fiévet, Size-dependent Magnetic properties of $CoFe_2O_4$ nanoparticles prepared in polyol, Chem. Mater., to be submitted.
(15) Ammar, S.; Helfen, A.; Jouini, N.; Fiévet, F.; Villain, F.; Rosenman, I.; Danot, M.; Molinié, P. *J. Mater. Chem.* **2001**, *10*, 186.
(16) (a) Carunti, D.; Remond, Y.; Chou, N. H.; Jun, M. J.; Carunti, G.; He, J.; Goloverda, G.; O'Connor, C.; Kolesnichenko, V. *Inorg. Chem.* **2002**, *41*, 6137. (b) Chkaoundali, S.; Ammar, S.; Jouini, N.; Fiévet, F.; Richard, M.; Villain, F.; Grenèche, J.-M.; Danot, M.; Molinié, P. *J. Physics: Condens. Mater.* **2004**, *16*, 4357.

Table 1. Main Structural and Microstructural Characteristics of the As-Produced and Subsequently Heated $Ni_{1-x}Zn_xFe_2O_4$ (x = 0.2 and 0.4) Particles

heating treatment	x	a_{nano}/Å	$\langle L_{XRD}\rangle$/ nm	$\langle \varepsilon^2\rangle^{1/2}$	$\langle D_{MET}\rangle$/ nm	σ/nm
as-produced	0.2	8.360(5)	7.6	0.0048	5.3	0.6
	0.4	8.380(5)	6.8	0.0061	5.7	0.8
heated at 400 °C	0.2	8.362(4)	12.6	0.0043	9.5	1.9
	0.4	8.380(8)	13.5	0.0037	8.9	2.2
heated at 600 °C	0.2	8.362(1)	29.5	0.0018	20.6	4.5
	0.4	3.381(1)	39.9	0.0013	22.1	5.0
heated at 800 °C	0.2	8.362(1)	111.5	0.0004	68.0	13.2
	0.4	3.381(1)	132.2	0.0003	70.5	15.0

which permits the preparation of size calibrated in the nanometer scale, monodisperse, almost isotropic in shape, nonagglomerated, and highly crystallized ferrite particles.[15,16] The as-prepared particles were subsequently heated at different temperatures, namely 400, 600, and 800 °C, and they were deeply characterized using X-ray diffraction (XRD), extended X-ray absorption fine structure spectroscopy (EXAFS), Transmission electron microscopy (TEM), dc and alternating current (ac) magnetometry, and ^{57}Fe Mössbauer spectrometry.

Experimental Section

1. Synthesis. The chemical reagents used in this study are anhydrous ferrous acetate, dihydrate zinc acetate, and tetrahydrate Nickel acetate salts and diethyleneglycol (DEG) solvent purchased from ACROS. All chemicals are analytical grade and used without further purification. First the salts are dissolved in the polyol solvent to reach a total iron concentration of 0.2 M. The nominal molar ratio Ni/Zn was varied in order to produce the solid solution $Ni_{0.8}Zn_{0.2}Fe_2O_4$ and $Ni_{0.6}Zn_{0.4}Fe_2O_4$. The hydrolysis ratio, h, defined by the water to metal molar ratio, was fixed to 12.[17] The mixture was then refluxed at a rate of 6 °C·min^{-1} up to the boiling temperature under mechanical stirring for about 3 h. A dark brown magnetic powder was then separated from the supernatant by centrifugation, washed with ethanol, and then dried in air at 50 °C.

The as-prepared powders were then subsequently heated at different temperatures, 400, 600, and 800 °C, for 2 h to prepare a series of annealed samples. At some temperatures, the annealing time was varied up to 12 h. It has found that at 600 °C, for instance, the particle size is independent of the annealing time from 2 to 12 h and the magnetic properties of all samples are almost the same. For this reason, we will focus our study on the samples heated for 2 h at different temperatures.

Hereafter, all the prepared samples are designed by their zinc content and their annealing temperature (see Table 1).

2. Characterization Techniques. The powders were characterized by XRD on a PANalytical X'pert Pro in the 15−120 2θ (deg) range with a scan step of 0.05°, using the Co Kα radiation (λ = 0.1789 nm). The cell parameters of the produced phases were deduced from the diffraction peak positions using Rietveld refinements. The crystallite mean size $\langle L\rangle$ was deduced from the XRD line integral breadth β using a Warren−Averbach method-based analysis.[18] These refinements were computationally performed by means of the MAUD program.[19]

TEM and HRTEM observations were carried out on a JEOL 2100F microscope operating at 200 kV, equipped with a field emission gun, a high resolution UHR pole piece, and a Gatan US4000 charge-coupled device (CCD) camera. The particle size distribution was obtained from the TEM images using a digital camera and the SAISAM software (Microvision Instruments), calculating the surface-average particle diameter through a statistical analysis obtained by counting about 400 particles considering a spherical particle shape. Elemental mapping were performed using X-ray energy dispersive spectroscopy (XEDS) analyses using a JEOL detector coupled with a scanning TEM device. Using the three-window technique,[20] energy filtered TEM (EFTEM) was performed with a GATAN Imaging filter 2001.

A MPMS-5S super quantum interference device (SQUID) magnetometer was used for magnetic characterization in the 4−330 K temperature range. The thermal zero-field-cooling (ZFC) and field-cooling (FC) dc-susceptibility, χ, variations were measured in a magnetic field of 200 Oe. The ZFC isothermal dc-magnetization was also measured at 5 and 300 K by cycling the magnetic field, H, between +50 and −50 kOe. The in-phase (χ') and out-of-phase (χ'') components of the ac-susceptibility were also measured at different frequencies with a magnitude of 1 Oe.

^{57}Fe Mössbauer spectra were recorded using a ^{57}Co/Rh γ-ray source mounted on an electromagnetic drive and using a triangular velocity form. They were obtained at 300 K and at 77 K in a zero magnetic field and at 10 K in an 8 T field oriented parallel to the γ-beam. In all the cases, the hyperfine structure was modeled by a least-squares fitting procedure involving Zeeman sextets and quadrupolar doublets composed of Lorentzian lines. The isomer shift values (IS) were referred to α-Fe at 300 K. The samples consist of a thin layer of about 40 mg of the powdered compounds located in sample holder.

EXAFS data were collected at 77 K for the Ni and Zn K edges of the particles using a transmission mode detection scheme with a Si(111) two-crystal monochromator on the XAFS beamline of the ELETTRA storage ring at the Italian facility (Trieste). The samples were ground and homogeneously dispersed in cellulose pellets. EXAFS data were analyzed using the "EXAFS pour le Mac" software package[21] with calculated amplitude and phase shift functions using the Feff7 program.[22]

Results

1. Chemical Analysis. XEDS analysis performed on all the produced powders and the subsequently heated ones shows that the Ni/Fe and Zn/Fe atomic content ratios are very close to the nominal ones in good agreement with the formula $Ni_{1-x}Zn_xFe_2O_4$ x = 0.2 and 0.4. Chemical analysis reveals that the as-prepared particles contain a small carbon content estimated at about 1.5 wt %. Such a carbon contamination which is frequently observed in oxide particles prepared in a polyol medium is due to acetate and polyol molecules adsorbed at the surface of

(17) Beji, Z.; Smiri, L.; Ben Chabane, T.; Ammar, S.; Jouini, N.; Fiévet, F.; Grenèche, J.-M. *Phys. Sol. Stat. A* **2006**, *203*, 504.
(18) Klug, H. P.; Alexander, L. E. *X-Ray Diffraction Procedures*; John Wiley: NewYork, 1974.
(19) Lutterotti, L.; Matthies, S.; Wenk, H. R. *IUCr: Newslett. Commission on Powder Diffraction* **1999**, *21*, 14.
(20) Kundmann, M. K.; Krivanek, O. L. *Microscopy, Microanal. Microstruct.* **1991**, *2*, 245.
(21) Michalovich, A. In *Logiciels pour la chimie*; La société Française de Chimie: Paris, 1991.
(22) Rehr, J. J.; Mustre de Leon, J.; Zabinsky, S. I.; Albers, R. C. *J. Am. Chem. Soc.* **1991**, *113*, 5135.

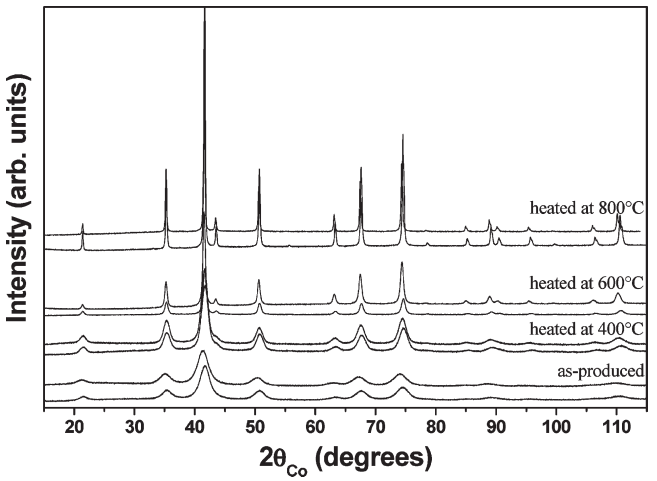

Figure 1. XRD patterns of the as-produced and subsequently heated at 400, 600, and 800 °C $Ni_{1-x}Zn_xFe_2O_4$ ($x = 0.2$ and 0.4) particles.

the particles.[15,23] After heating at 400 °C, the carbon content decreases to about 0.2 wt % due to the loss of most part of the adsorbed organic species and vanishes to zero after heating at higher temperatures.

2. X-ray Diffraction Analysis. The XRD patterns of all the samples are indexed in a pure spinel-like structure (Figure 1). There is no evidence of any extra phases such as hematite, α-Fe_2O_3, or simple NiO and ZnO oxides. The as-prepared powders appear crystallized since all the broadened reflection peaks of the spinel planes can be observed in the XRD patterns. Nevertheless, the increment of the calcination temperature induces more crystalline products, as can be seen from the sharp diffraction peaks and line narrowing features for the samples annealed at 400, 600 and 800 °C. The enhancement of the crystallinity is correlated to the crystal size increase.

Rietveld refinements using the MAUD program considering a pseudo-Voigt diffraction line profile allowed us to determine the mean cell parameter value. From data listed in Table 1, one observes that the cell parameter varies linearly with the composition in agreement with Vegard's law. In addition, the refined values are in agreement with those reported for the bulk ferrites[24] and remain almost the same for a given composition whatever the heating temperature of the sample. On the contrary, the average crystalline size is rather independent of the zinc content but dependent on the heating temperature. Obviously, it increases progressively when going from the as-prepared to the annealed at 800 °C powders while the average microstrain deformation decreases slightly from about $5-6 \times 10^{-3}$ to $3-4 \times 10^{-4}$ (see Table 1). This analysis shows that the prepared nickel–zinc ferrite powders are constituted by almost strain-free nanocrystals with an average crystal size independent from the zinc content but dependent on the heating temperature.

3. Electron Microscope Study. TEM measurements allow a more detailed analysis of the particle size and shape. The as-prepared powders consist of nonagglomerated nanometer-sized particles (Figure 2a). The particles do not have peculiar shape, and their mean diameter is about 6 nm, in good agreement with the average crystallite size inferred from XRD analysis, suggesting that they are single crystals. This is confirmed by high resolution observations. A high crystalline quality of the as-prepared particles can be also noticed. This is unambiguously related to the synthesis conditions offered by the polyol process. The thermal conditions are here close to the hydrothermal ones (reflux at 160−170 °C for several hours) which is well established to favor good crystallinity and accordingly improve magnetic properties.

After heating up to 400 °C, the TEM images show more agglomerated particles. The particles are still nanometer-sized with a quasi-spherical shape (Figure 2b); however, their average diameter increases up to about 10 nm, two times higher than that of the as-prepared particles (Table 1). This value is close to the average crystallite size deduced from XRD suggesting that the heated particles remain still single crystals. This observation agrees well with the fact that the reduction of the distance between particles occurs by the decomposition of residual organic coating. As a consequence, groups of 5−6 nm sized particles just touching each other coalesce: neighboring nanoparticles fuse side-on. Growth, by both interdiffusion and migration between the nanoparticles, results from the supplement of thermal activation energy, leading thus to larger single crystals. In these conditions, the large particles share common interfaces (Figure 2b).

The effect of the heating process is more pronounced for higher temperature. For 600 °C, larger crystals are observed (Figure 2c). Moreover, it appears that the crystals may have defined crystallographic relationships. Figure 3a shows two crystals having different orientation with respect to the electron beam, i.e. respectively [114] and [110], but with a common ⟨110⟩ direction (Figure 3b). A stereographic projection analysis reveals that these two crystals have a common (111) plane which is known to be a twininng plane in the magnetite spinel structure (Figure 3c and d). Such a structural feature implies a possible recrystallization process induced by the annealing. The strong impact of heating is clearly shown.

For 800 °C heating, large particles are observed with frequent agglomeration of large particles (Figure 2d). Classical polygonal grain and grain boundary morphologies can be observed in agreement with a progressive sintering process.

Size distribution analysis of the large particles shows that they are less uniform in size than the initial ones (Figure 2). The standard deviation of the diameter represents ~25% of the average diameter for the particles heated at 400 °C while it does not exceed ~15% for the as-prepared ones. This trend is confirmed by comparing the

(23) Boubekri, R.; Beji, Z.; Elkabous, K.; Herbst, F.; Viau, G.; Ammar, S.; Fiévet, F.; von Bardeleben, H. J.; Mauger, A. *Chem. Mater.* **2009**, *21*, 843.
(24) (a) Verma, A.; Goel, T. C.; Mendiratta, R. G.; Gupta, R. G. *J. Magn. Magn. Mater.* **1999**, *192*, 271.(b) Valenzuela, R. *Magnetic ceramics*; Cambridge University Press: Cambridge, 1994.

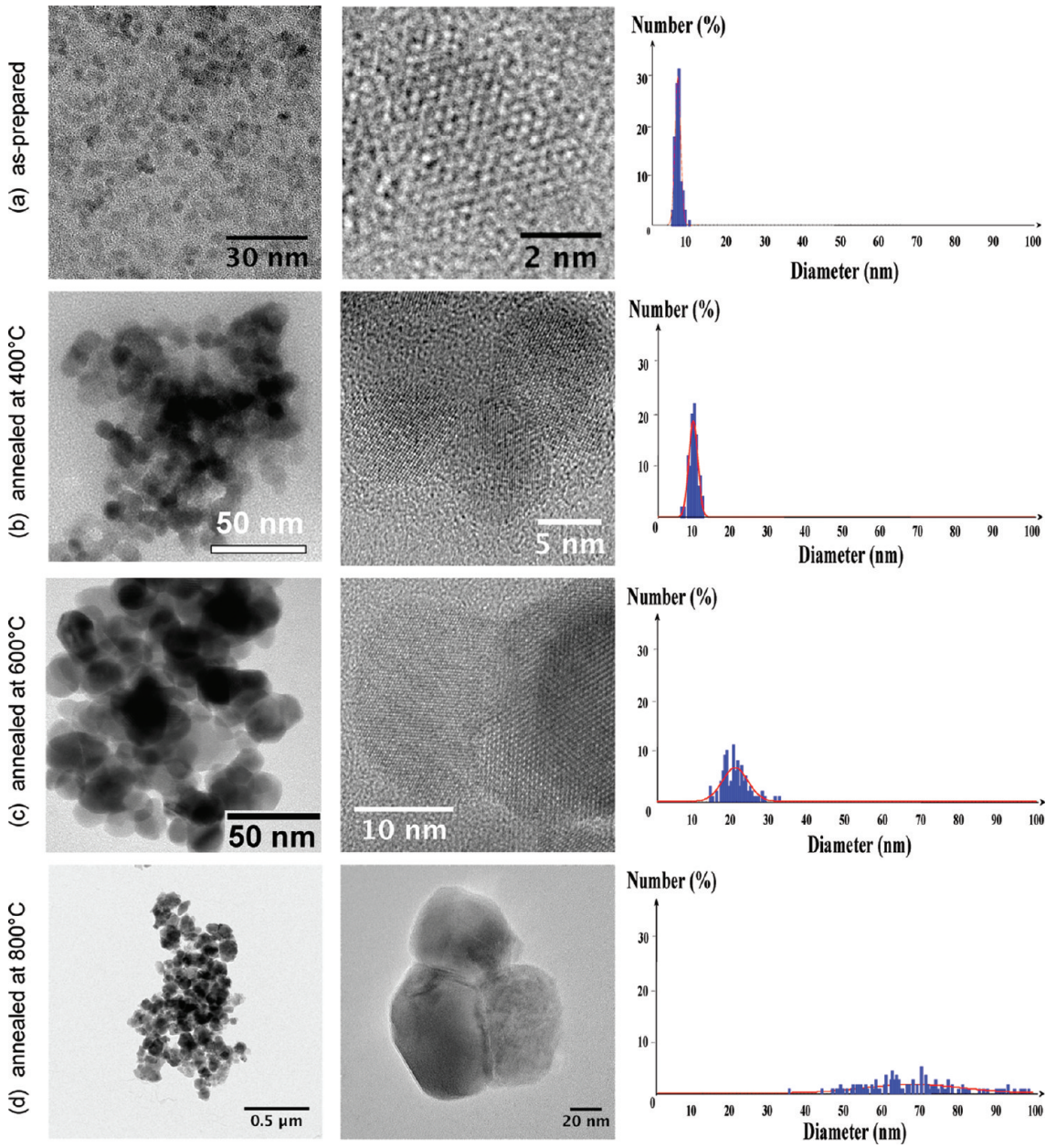

Figure 2. TEM images of a collection of as-produced (a) and subsequently heated at 400 (b), 600 (c), and 800 °C (d) $Ni_{0.8}Zn_{0.2}Fe_2O_4$. In each case, a zoom on one or more representative particles is given, as well the size distribution of the particles deduced from TEM images analysis.

TEM and HRTEM images of the samples annealed at higher temperatures. Indeed, the average particle diameter increases up to ~20 nm for the annealed ferrite samples at 600 °C and reaches about 60−70 nm for the annealed ones at 800 °C (see Table 1 and Figure 2). A progressive densification of the particles occurred by heating. These results implies that the heat energy supplied to the system not only induced the crystallization but also increased the surface energy of the particles favoring their aggregation inducing a significant effect on the magnetic properties of the particles. Nevertheless, the particles remain still single crystals, since their average diameter agrees well with the crystal size inferred from XRD analysis (Table 1). Note that the measured average diameter values for all the studied particles are largely lower than the critical diameter below which particles become single domains. This point must be underlined, because, as for the particles described in previous works and mentioned in the literature, the particles studied here can be assumed to be in their magnetic single-domain regime.

In order to verify the chemical homogeneity of the sample, we performed EFTEM imaging and/or XEDS mapping. Figure 4a and b exhibits TEM micrographs of a quite representative area of the $Ni_{0.8}Zn_{0.2}Fe_2O_4$ sample heated at 400 and 800 °C, respectively, as well as their Fe, Ni, and Zn mapping. These images show that, despite a weak contrast on zinc because of its low concentration, Fe, Ni, and Zn are localized almost uniformly all over the material, indicating that the particles do not exhibit chemical segregation. There is neither a zinc, nor nickel, concentration gradient in each observed particle or from

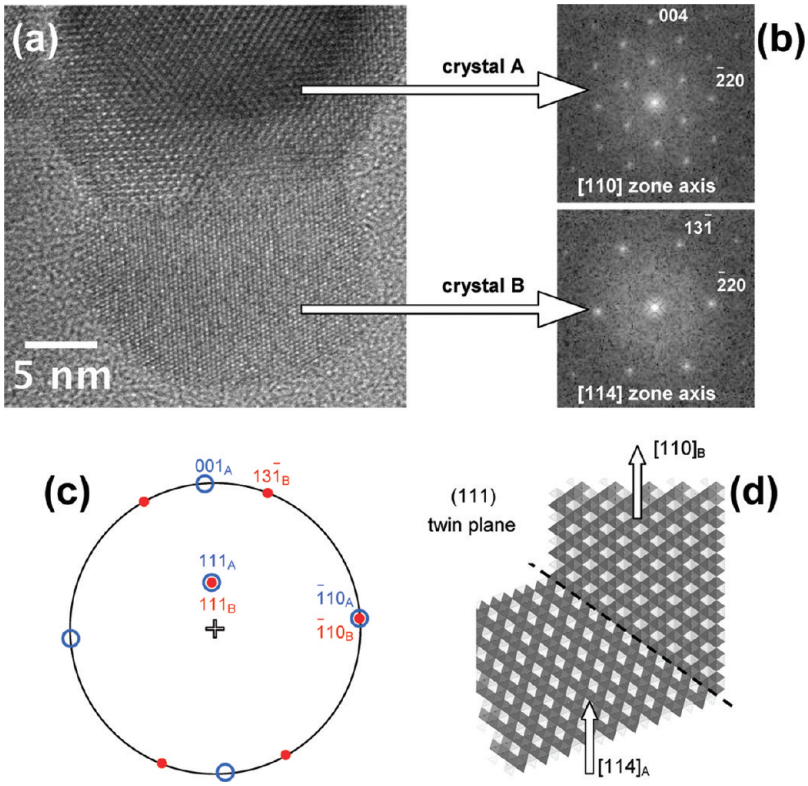

Figure 3. Structural analysis of the $Ni_{0.8}Zn_{0.2}Fe_2O_4$ nanocrystals heated at 600 °C.

one particle to another one. We assumed that the sample heated at 600 °C is also homogeneous, since 600 °C is an intermediary temperature between 400 and 800 °C. We did not succeed to perform the same experiments on the as-prepared particles: indeed, due to their very reduced size (~5 nm), almost close to the spatial resolution offered by the used energy mapping analyzer probe (~1 nm), we were not able to appreciate unambiguously the chemical homogeneity of the as-prepared particles. Hence, we acceded to this information indirectly using magnetic measurements. This point will be discussed in a further section.

3. EXAFS Analysis. The local environment of nickel and zinc ions was investigated using X-ray absorption spectroscopy. The Fourier-transformed (FT) EXAFS K−Ni and K−Zn edges data of the as-prepared and subsequently heated at 400 °C $Ni_{1-x}Zn_xFe_2O_4$, $x = 0.2$ and 0.4, nanoparticles were plotted and compared to that of standard $NiFe_2O_4$ and $ZnFe_2O_4$. For bulk $NiFe_2O_4$, the FT curve consists of three peaks at 1.67, 2.58, and 3.10 Å in the 0−4 Å *R*-range (phase shift uncorrected). The first peak corresponds to Ni−O bonds, the second to the Ni−M_B, and the third to Ni−M_A and Ni−O, where M_B is the metal ion located in B (octahedral) spinel sites and M_A is that located in A (tetrahedral) ones. By analogy, it is possible to identify the different coordination shells of nickel atoms in the nanoparticles (Figure 5). Three peaks are clearly resolved. The positions of the FT Ni EXAFS peaks in our material are close to those observed with standard $NiFe_2O_4$ (inverse spinel); however, their amplitudes are different. First, the total FTs have a reduced amplitude suggesting that the as-prepared particles are small, in agreement with XRD and TEM results. The surface nickel ions of the particles have nearest metallic neighbors on one side none on the other side. Note that the peaks in the attendant Fourier transforms do not exhibit a significant decreasing attenuation with increasing particle size, namely from the as-prepared particles to the annealed ones at 400 °C as it is usually the case.[26] Quite independently of the zinc content, we can observe only a slight increase in the intensity of the second, third, and the other peaks in the FT of the particles heated at 400 °C compared to that of the as-prepared ones. This reflects a slight change in the influence from the surface environment despite particle size increase. The second difference is related to the intensity of the third peak whose center appears at 3.10 Å which mainly corresponds to the tetrahedral/tetrahedral and tetrahedral/octahedral metal correlations. Its amplitude is enhanced compared to that of the bulk standard suggesting that the absorbing species reside partly in the tetrahedral spinel sites. Such behavior was already observed for partially inversed Zn-substituted $NiFe_2O_4$ nanocrystalline films.[25] Note that, by comparison, the intensity ratio between this FT peak and that centered at 2.58 Å is less important in the heated at 400 °C $Ni_{1-x}Zn_xFe_2O_4$, $x = 0.2$ and 0.4, particles than in the as-prepared ones. This suggests that the structural deviation suspected in the studied particles must be less important

(25) Harris, V. G.; Koon, N. C.; Williams, C. M.; Zhang, Q.; Abe, M.; Kirkland, J. P.; McKeown, D. A *IEEE. Trans. Magn.* **1995**, *31*, 3473.
(26) Nordhei, C.; Ramstad, A. L.; Nicholson, D. G. *Phys. Chem. Chem. Phys.* **2008**, *10*, 1053.

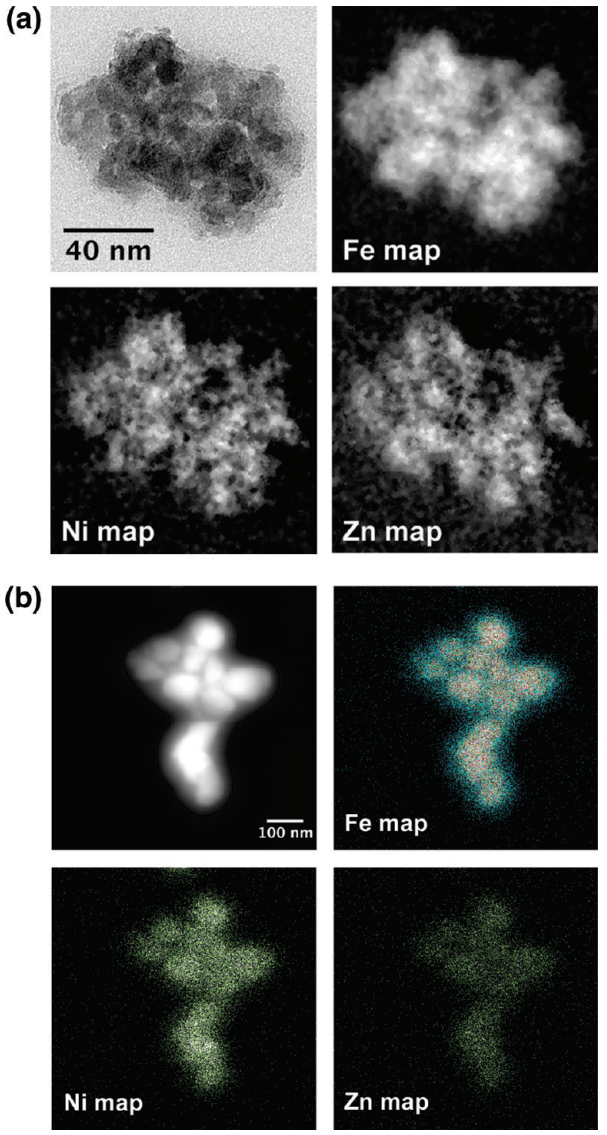

Figure 4. TEM images and XEDS energy mapping of a collection of subsequently heated $Ni_{0.8}Zn_{0.2}Fe_2O_4$ nanoparticles at 400 (a) and 800 °C (b).

in the heated samples. The structural parameters obtained by modeling the first coordination sphere at the Ni K-edge, in a simple scattering scheme, confirm this tendency. The inverse Fourier transform of the first peak at the Ni K-edge is well fitted considering both Ni_A-O and Ni_B-O pair contributions, where A and B labels correspond to the Ni^{2+} cations in tetrahedral and octahedral spinel sites, respectively, for all studied samples (Figure 7). Obviously, the intermediate N value, which measures the number of oxygen atoms at 2.05 Å, obtained for the Ni_B-O pair compared to the bulk-like $Ni_{1-x}Zn_x$-Fe_2O_4 ferrite one allows us to estimate the proportion of nickel atoms in each spinel site, which is about 15% in A and 85% in B sites in the as-prepared particles and 7% in A and 94% in B sites in the heated ones at 400 °C (Table 2). These ratios do not depend on the composition of the particles, since we obtained the same results for both $x = 0.2$ and 0.4 samples.

At the Zn K-edge, a great proximity between the overall FT profiles of the samples and the standard $ZnFe_2O_4$ is observed, where Zn cations occupy exclusively tetrahedral sites (Figure 6). Nevertheless, the intensity of the peak centered at 3.1 Å, corresponding to the distance between the Zn ions and their second nearest metallic neighbors, is reduced in the case of as-prepared nanoparticles (Figure 6). This feature was assumed to be due to both the nanocrystalline character of the particles and the partial transfer of Zn^{2+} cations from tetrahedral into octahedral spinel sites. Indeed, least-squares modeling using single scattering Zn EXAFS simulation on the first filtered Zn FT peak corresponding to the Zn−O shells (Figure 8) showed that about 30% of Zn^{2+} cations are octahedrally coordinated in the as-prepared particles whatever their zinc content and only 5% are in the annealed ones at 400 °C (Table 2).

Unfortunately the samples heated at higher temperatures, namely 600 and 800 °C, were not analyzed. Nevertheless it is possible to extrapolate the obtained results to these samples. Indeed, EXAFS refinements indicate that the structure of the as-prepared particles due to their highly reduced size and their moderate temperature synthesis conditions differs from that of their bulk counterparts. They also showed that the deviation from the thermodynamic stable structure is less important in the heated samples at 400 °C. The tetrahedrally coordinated Ni^{2+} and octahedrally coordinated Zn^{2+} concentrations are divided by two and five, respectively, from the as-prepared particles to the annealed ones. One can conclude that heating offers thermodynamic conditions where the degree of structure inversion, in the spinel lattice, becomes only dependent on the ionic radius, the configuration of the cations, and their relative stabilization energies in the tetrahedral and octahedral electrostatic fields. In these conditions, the heated samples at 600 and 800 °C must exhibit a close to bulk spinel structure.

EXAFS measurements evidenced that the preference of Ni^{2+} ions for octahedral sites is stronger than the preference of Zn^{2+} ions for tetrahedral sites, and this preference is enhanced when the particles are annealed. Such a behavior already predicted by thermodynamic calculations[51,52] was suggested to be due to a "quicker migration" of nickel ions compared to zinc ions, to the sites in which they are stable.[53]

4. Mössbauer Spectrometry Analysis. The room temperature Mössbauer spectra of the samples show a systematic variation with heating temperature increase (Figure 9). For the as-prepared particle, the spectra consist only of a central doublet, while the particles annealed at high temperatures show the presence of distinct, but still broadened, line magnetic sextet. As observed from both XRD and TEM studies, the particle size increases with increase in annealing temperature. Hence the systematic variation in the Mössbauer spectra with annealing temperature can be correlated to the particle size. If the crystallite sizes are so small that the thermally induced energy fluctuations can overcome the anisotropy energy and change the direction of the magnetization of a particle from one easy axis to

Table 2. EXAFS Results at the Ni and Zn K-Edges of As-Produced and Subsequently Heated at 400 °C $Ni_{1-x}Zn_xFe_2O_4$ (x = 0.2 and 0.4) Particles[a]

			N		R (Å)		σ		ΔE (eV)		%	
K-edge	heating treatment	x	site A	site B	site A	site B	site A	site B	site A	site B	site A	site B
Ni	as-produced	0.2	**0.66**	**5.14**	**1.93**	**2.04**	**0.089**	**0.058**	**1.9**	**5.4**	**16**	**86**
		0.4	**0.53**	**4.96**	**1.93**	**2.05**	**0.061**	**0.056**	**8.0**	**4.9**	**13**	**83**
	heated at 400 °C	0.2	**0.28**	**5.56**	**1.94**	**2.05**	**0.049**	0.055	3.0	5.5	**7**	**93**
		0.4	**0.28**	**5.39**	**1.94**	**2.06**	**0.049**	0.060	5.3	7.8	**7**	**92**
Zn	as-produced	0.2	**2.96**	**1.71**	**1.94**	**2.04**	**0.046**	**0.086**	**6.5**	**12.1**	**74**	**28**
		0.4	**2.75**	**1.98**	**1.95**	**2.05**	**0.041**	**0.087**	**9.7**	**7.9**	**70**	**30**
	heated at 400 °C	0.2	**3.70**	**0.33**	**1.93**	**2.07**	**0.055**	**0.040**	**7.4**	**12.0**	**92**	**6**
		0.4	**3.80**	**0.27**	**1.95**	**2.08**	**0.055**	**0.049**	**10.4**	**10.5**	**95**	**5**

[a] N is the number of backscatterers (the relative precision is about 15%) at a distance R (the absolute precision is about 0.02 Å) from the central atom, and σ is the Gaussian Debye−Waller factor associated with R. The energy threshold, E_0, taken at the first inflection of the Ni absorption edge is corrected in the fitting procedure by the ΔE_0 parameter.

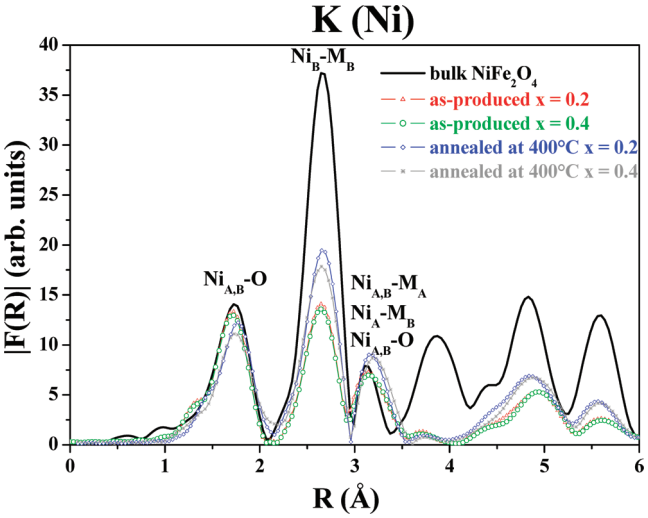

Figure 5. Modulus of the k^3-weighted Fourier transform of the Ni K-edge EXAFS data for the as-produced and subsequently heated at 400 °C $Ni_{1-x}Zn_xFe_2O_4$ (x = 0.2 and 0.4) particles compared to that recorded for bulk $NiFe_2O_4$.

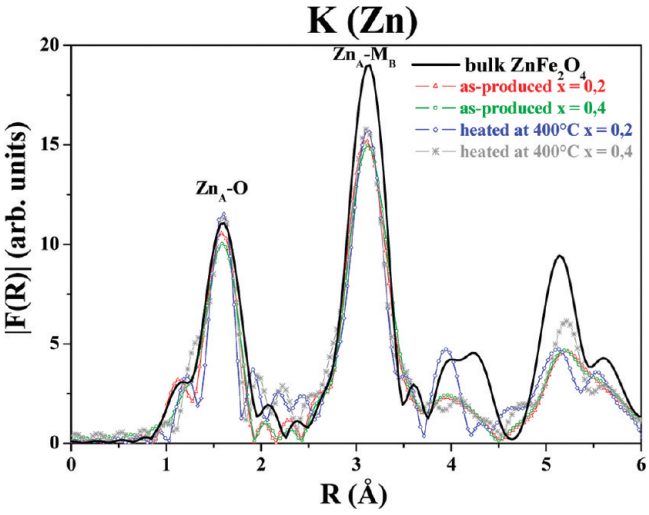

Figure 6. Modulus of the k^3-weighted Fourier transform of the Zn K-edge EXAFS data for the as-produced and subsequently heated at 400 °C $Ni_{1-x}Zn_xFe_2O_4$ (x = 0.2 and 0.4) particles compared to that recorded for bulk $ZnFe_2O_4$.

another, superparamagnetic relaxations are observed in the Mössbauer spectrum and the magnetic sextet collapses into a doublet. The relaxation time τ is given

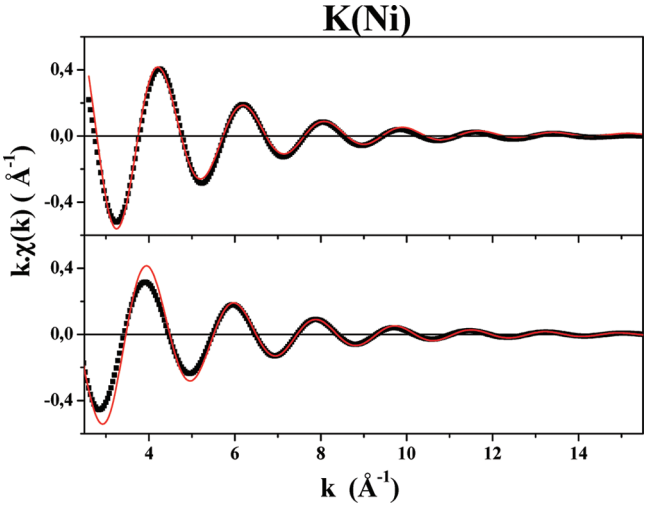

Figure 7. Inverse Fourier transform of the first peak at the Ni K-edge for the as-produced and the subsequently heated at 400 °C $Ni_{0.8}Zn_{0.2}Fe_2O_4$ particles. The red continuous line corresponds to a fit considering both octahedral and tetrahedral coordination spheres for each absorbing cation.

by the expression:

$$\tau = \tau_0 \exp\left(\frac{KV}{k_B T}\right) \quad (1)$$

where K is the effective anisotropy energy constant, V is the particle volume, k_B is Boltzmann's constant, and T is the temperature. When τ is less than the Larmor precession time, τ_L, a superparamagnetic doublet is observed in the Mössbauer spectrum. The occurrence of a single doublet in the spectra of the as-prepared samples has to be attributed to superparamagnetic relaxation due to the extremely small size of noninteracting or just weakly interacting particles. For the annealed samples, the particle size becomes large enough to prevent the flipping of magnetic moments, and the subsequent collapse of the magnetic hyperfine sextets into doublets, due to thermal agitation, disappears progressively. The spectra would be thus fitted with two doublets, corresponding to the tetrahedrally and octahedrally coordinated iron cations, for the as-prepared particles, with a combination of two doublets and two sextets for the particles annealed at 400 °C and only with two sextets for the particles annealed at higher temperatures, namely 600 and 800 °C. It is now

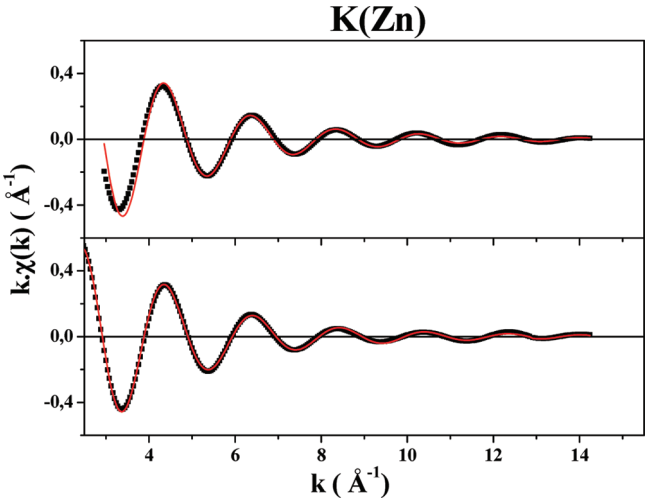

Figure 8. Inverse Fourier transform of the first peak at the Zn K-edge for the as-produced and the subsequently heated at 400 °C $Ni_{0.8}Zn_{0.2}Fe_2O_4$ particles. The red continuous line corresponds to a fit considering both octahedral and tetrahedral coordination spheres for each absorbing cation.

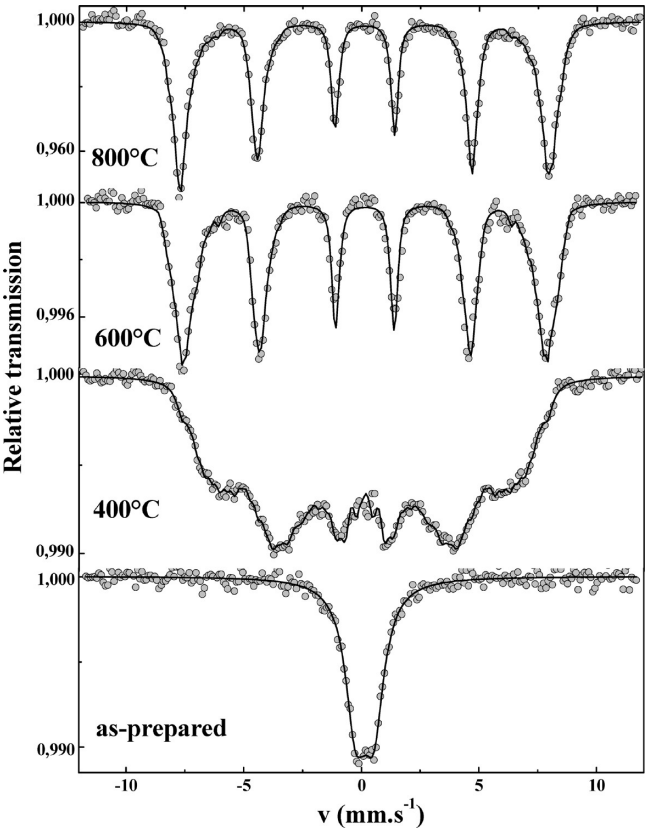

Figure 9. ^{57}Fe Mössbauer spectra recorded at 300 K on the as-produced and subsequently heated at 400, 600, and 800 °C $Ni_{0.8}Zn_{0.2}Fe_2O_4$ particles.

important to emphasize that the quantitative description remains delicate because the relative absorption areas are related to the linewidths and the line broadening observed here causes a lack of resolution. The best procedure for an optimized quantitative analysis would consist of applying an external magnetic field, in order to split the broadened line sextet into two well-resolved sextets with respect to the ferrimagnetic structure of the oxides. As atomic

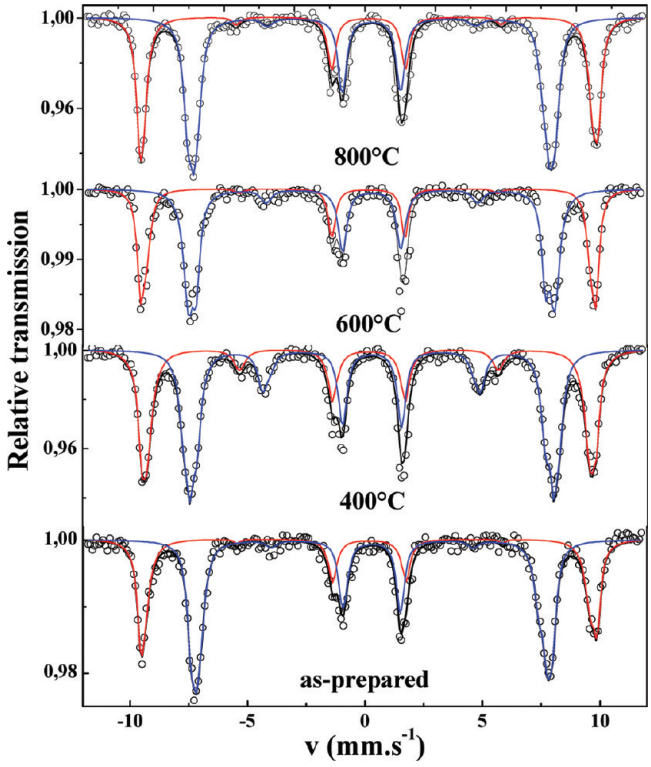

Figure 10. In-field-Mössbauer spectra recorded at 10 K under an applied magnetic field of 8 T on the as-produced and subsequently heated at 400, 600, and 800 °C $Ni_{0.8}Zn_{0.2}Fe_2O_4$ particles.

substitution gives rise to different environments for Fe sites, each component does result from the superposition of sextets with narrow lines and the profile could be estimated from the refinement of in-field Mössbauer spectra. Figure 10 illustrates the spectra recorded at 10 K under a magnetic field of 8 T applied parallel to the γ-beam in the case of the $x = 0.2$ samples. They are unambiguously consistent with a ferrimagnetic structure: the refinement allows us to now attribute clearly the two sextets to tetrahedral (A) and octahedral (B) Fe^{3+} sites, according to the values of the isomer shift and to estimate accurately the atomic Fe_A^{3+}/Fe_B^{3+} population ratio (Table 3). These ratios are found to be significantly different from that observed for bulk $Ni_{1-x}Zn_xFe_2O_4$ materials for the as-prepared particles and closer for the annealed ones particularly for the samples annealed at 600 and 800 °C (Table 3). Note that the recorded spectra on all studied samples do not evidence at all the presence of Fe^{2+} ions (the limit of detection is usually estimated to be about 1%).

The in-field Mössbauer spectra analysis results combined to that of EXAFS spectra, allow the appreciation of the cation distribution into the spinel lattice and the description of the local structure of the all studied samples through the chemical formulas given in Table 4. These formulas show clearly that Ni^{2+}, Zn^{2+}, and Fe^{3+} cations occupy simultaneously the tetrahedral and octahedral sites of the spinel structure in the as-prepared particles with decreasing tetrahedrally coordinated Ni^{2+} cation and octahedrally coordinated Zn^{2+} cation concentrations with a heating temperature increase. At 600 and 800 °C,

Table 3. In-Field Mössbauer Fitted Parameters of the As-Produced and Subsequently Heated at 400, 600, and 800 °C $Ni_{1-x}Zn_xFe_2O_4$ (x = 0.2 and 0.4) Particles

heating treatment	x	site	δ/mm·s^{-1} ± 0.01	2ε/mm·s^{-1} ± 0.01	B_{eff}/T ± 2	B_{hyf}/T ± 2	θ/deg ± 10	$Fe_{A,B}^{3+}/Fe_{total}^{3+}$ ± 0.01
as-produced	0.2	Fe_A^{3+}	0.35	−0.02	59.2	51.3	10	0.39
		Fe_B^{3+}	0.47	−0.03	46.0	53.9	13	0.61
	0.4	Fe_A^{3+}	0.34	0.00	59.8	51.8	4	0.32
		Fe_B^{3+}	0.48	0.00	45.5	53.4	10	0.68
heated at 400 °C	0.2	Fe_A^{3+}	0.34	−0.02	58.5	52.1	34	0.42
		Fe_B^{3+}	0.47	−0.03	47.6	54.8	27	0.58
	0.4	Fe_A^{3+}	0.34	0.03	59.1	51.9	25	0.34
		Fe_B^{3+}	0.48	0.01	46.5	53.6	29	0.66
heated at 600 °C	0.2	Fe_A^{3+}	0.35	0.00	59.2	51.5	13	0.39
		Fe_B^{3+}	0.48	−0.02	47.4	55.0	20	0.61
	0.4	Fe_A^{3+}	0.35	−0.00	59.5	51.5	18	0.33
		Fe_B^{3+}	0.50	−0.03	45.9	53.8	11	0.67
heated at 800 °C	0.2	Fe_A^{3+}	0.36	0.00	59.6	51.4	15	0.41
		Fe_B^{3+}	0.49	0.00	47.1	54.2	14	0.59

Table 4. Cation Distribution Deduced From EXAFS and Mössbauer Analysis of the As-Produced and Subsequently Heated $Ni_{1-x}Zn_xFe_2O_4$ (x = 0.2 and 0.4) Particles

heating treatment	x	distribution of cations
as-produced	0.2	$(Zn_{0.12}Ni_{0.10}Fe_{0.78})[Ni_{0.70}Zn_{0.08}Fe_{1.22}]O_4$
	0.4	$(Zn_{0.26}Ni_{0.08}Fe_{0.64})[Ni_{0.52}Zn_{0.14}Fe_{1.36}]O_4$[a]
heated at 400 °C	0.2	$(Zn_{0.18}Ni_{0.02}Fe_{0.84})[Ni_{0.78}Zn_{0.02}Fe_{1.16}]O_4$[a]
	0.4	$(Zn_{0.38}Ni_{0.04}Fe_{0.68})[Ni_{0.56}Zn_{0.02}Fe_{1.32}]O_4$[a]
heated at 600 °C	0.2	$(Zn_{0.20}Fe_{0.78})[Ni_{0.80}Fe_{1.22}]O_4$[a]
	0.4	$(Zn_{0.40}Fe_{0.66})[Ni_{0.60}Fe_{1.44}]O_4$[a]
heated at 800 °C	0.2	$(Zn_{0.20}Fe_{0.82})[Ni_{0.80}Fe_{1.18}]O_4$[a]
	0.4	[b]

[a] The given compositions are only based on the analysis of EXAFS and Mössbauer spectra. The obtained results contain a certain accuracy. So, the proposed formulas do not traduce at all any nonstoichiometry. [b] Mössbauer experiments are still in progress for these samples.

these cations would be exclusively octahedrally and tetrahedrally coordinated, respectively.

In addition, the in-field Mössbauer spectrum allows an estimation of both the effective fields B_{eff} and the angles θ of the two types of sites, where B_{eff} corresponds to the vectorial sum of the hyperfine field B_{hyf} and the applied field B_{app} and θ to the angle defined by the directions of the effective field for both tetrahedral and octahedral iron components and the γ-beam direction. The hyperfine field values for Fe^{3+} in tetrahedral and octahedral site are thus about 51 and 54 T, respectively, except for the particles annealed at 400 °C, where B_{hyf} values are quite different, about 52 and close to 55 T for the A and B sites, respectively (Table 3). The previous values are close to the reported ones for bulk $Ni_{1-x}Zn_xFe_2O_4$,[27] while the former are surprisingly larger.

Close inspection of the in-field spectra shows that the second and fifth lines have clearly a nonzero intensity for the particles annealed at 400 °C. The as-prepared ones and the heated ones at higher temperature exhibit a zero or close to zero second and fifth line intensity. Usually, when these peaks are distinctly observed they evidence a canted structure for Fe^{3+} magnetic moments with respect to the applied field in both A and B sites. Indeed, the in-field Mössbauer measurements show that the canting angle is close to zero ($\leq$10) for Fe^{3+} in tetrahedral sites and very low (10−13°) for Fe^{3+} in octahedral sites in the as-prepared particles despite their very reduced size (about 5 nm). The canting angle is also very low for both octahedrally and tetrahedrally coordinated Fe^{3+} in the heated samples at 600 and 800 °C, while it is significantly higher for the samples heated at 400 °C, reaching 34° for Fe^{3+} in A sites and 27° for Fe^{3+} in B sites. Theoretically, spin canting in such nanomaterials is likely attributed to (i) a chemical segregation leading to nanoparticles with a Yafet−Kittel-like ferrimagnetic Zn rich Ni−Zn ferrite core, with a composition close to $ZnFe_2O_4$, surrounded by a Néel-like ferrimagnetic Ni rich Ni−Zn ferrite shell, with a composition close to $NiFe_2O_4$, or inversely—the Zn rich part of the particles would exhibit a Yafet−Kittel canting due to the magnetic frustration resulting from the competition between A−B and B−B exchange interactions;[28] (ii) a surface effect related to the finite-size scaling which leads to a noncollinearity of magnetic moments on their surface due to broken exchange bonds at the external layer of the particles (the surface spin having nearest neighbors on one side, none on the other side)[29]—the particles could be described as consisting of ferrimagnetically aligned core spins and a spin-glass-like surface layer;[30] (iii) a poor crystallinity accompanied with great structural disorder which leads to noncollinearity of magnetic moments in their core due to break-up of magnetic exchange paths.[31] XRD and TEM analyses performed previously on all the studied samples have shown that the particles are well crystallized even the as-prepared ones and they are almost chemically homogeneous, at least the heated ones. In the present case, the spin canting is only clearly apparent for the intermediate sized particles produced by subsequent heating at 400 °C, which have not the higher atomic surface to volume ratio, suggesting that the surface effects are almost negligible or contribute differently in the magnetic behavior of the particles. It will be interesting to clarify this situation.

(27) Leung, L. K.; Evans, B. J.; Morrish, A. H. *Phys. Rev. B* **1973**, *8*, 29.
(28) Yafet, Y.; Kittel, C. *Phys. Rev.* **1952**, *87*, 290.
(29) Kodama, R. H.; Berkowitz, A. E.; McNiff, E. J.; Foner, J.; Foner, S. *J. Appl. Phys.* **1997**, *81*, 5552.
(30) Kodama, R. H. *J. Magn. Magn. Mater.* **1999**, *200*, 359.
(31) Morales, M. P.; Veintemillas-Verdaguer, S.; Montero, M. I.; Serna, C. J.; Roig, A.; Casas, L.; Martinez, B.; Sandiumenge, F. *Chem. Mater.* **1999**, *11*, 3058.

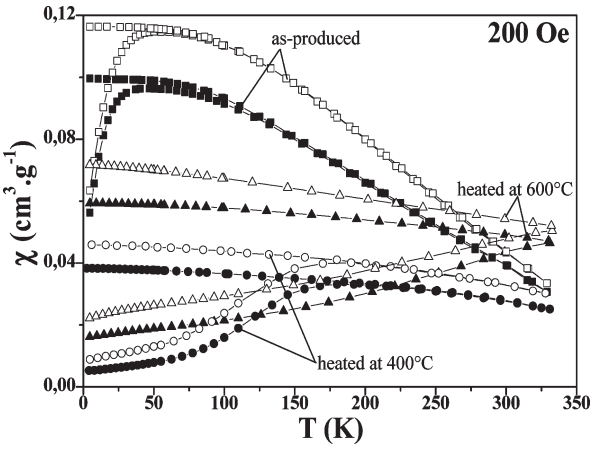

Figure 11. Thermal variation of the FC- and ZFC-susceptibility measured at 200 Oe on the as-produced and subsequently heated at 400 and 600 °C $Ni_{1-x}Zn_xFe_2O_4$ $x = 0.2$ (filled symbols) and $x = 0.4$ (empty symbols) particles.

5. Magnetic Measurements. The ZFC-FC thermal variation of the dc-susceptibility curves for varying x values is shown in Figure 11 for the as-prepared particles and the subsequently heated ones. These measurements were performed at a low field of 200 Oe in order to avoid the nonlinearity effect. The obtained curves are typical of superparamagnetic particles. The variation of the blocking temperature, T_B, conventionally measured at the maximum of the ZFC curve, as a function of zinc content is very weak. It is of about 47 and 53 K for $x = 0.2$ and 0.4, respectively. For each composition, T_B increases significantly when heating temperature increases. This increase is mainly due to the particle size increase. Moreover, the peak in the ZFC curve becomes broader with increasing heating temperature, namely particle size, which should indicate the presence of a broad distribution of relaxation times for the metastable magnetic states in relation with a less and less uniform particle size distribution. Note also that the measured T_B value on the heated particles at 600 and 800 °C is certainly higher than room temperature. The temperature range available on the used magnetometer for these measurements is limited to 52 °C (330 K), because the plastic sampling tube can fuse at higher temperature. We do not exactly observe a maximum in the ZFC-dc-susceptibility curves, but the general curve shapes suggest an average T_B value slightly higher than 330 K. The increase of the T_B value with the heating temperature, for a given zinc composition, can be also related to an enhancement of the strength of dipolar interactions. Indeed, previous experimental and theoretical works established that with increasing interparticle spacing, the maxima of the ZFC-dc-susceptibility curves related to the mean blocking temperatures T_B, shift toward lower temperatures and inversely decreasing interparticle spacing provides a T_B value increase.[35] TEM observations have shown that a partial densification of the powder take place with heating. The heating induced departure of the adsorbed organic species, from the surface of the as-prepared particles. The particles became more and more closer, aggregated, and then affected by the interparticle interactions. Usually, the strength of these interactions can be qualitatively measured by following the shape of the FC$-\chi(T)$ curves. An increase in the FC magnetization at low temperatures is observed for noninteracting particles and this tends to be reduced by the effect of the interactions.[32] When the interactions are so strong, a plateau is observed due to a collective behavior of the magnetic particles.[32] Unfortunately, the comparison between the measured FC magnetizations for the as-produced and the subsequently heated particles does not permit us to ascribe the FC magnetization feature to a different degree of interparticle interactions.

The change of the interparticle interaction strength can be visualized by plotting the thermal variation of the in-phase and out-of-phase χ' and χ'' components of the ac susceptibility at different alternative field frequencies ($\nu = 1$ and 1000 Hz). They exhibit a frequency dependent maximum (Figure 12). The temperature of the maximum (T_{max}) for each component increases with increasing frequency. Such behavior is usually observed in superparamagnetic particles.[33] The frequency shift per decade, of the maximum of out-of-phase ac susceptibility vs T, was used to calculate a quantity ϕ defined according the equation given above which usually permits to appreciate the strength of the interparticle magnetic interactions:[34]

$$\phi = (\Delta T_{max}/(T_{max}\Delta \log(2\pi\nu)) \quad (2)$$

ϕ is on the order of 0.09 for the as-prepared particles. This value is close to 10^{-1}, the minimal value for noninteracting superparamagnetic particles, suggesting that they are quite sufficiently distanced from each other through the sterical repulsions between the adsorbed organic species on their surface. Also, ϕ is on the order of 0.04 for the subsequently heated at 400 °C particles. This value is lower than the 10^{-1} limit and higher than the $5\ 10^{-3}$ one, which corresponds to the situation of strongly interacting superparamagnetic particles involving macro-spin glass behavior,[34] confirming the fact that these particles are more interacting than the previous ones. Note that these interactions induce also a decrease of the overall magnetization of the particles. If one compares the measured χ_{max} values, corresponding to the ZFC-χ values at T_B, for all the studied samples, one can observe that they are weakly dependent on Zn content for a given heating temperature but they are strongly dependent on the heating temperature for a given Zn content (Figure 11). They decrease from the as-produced particles to the heated ones at 400 °C, in agreement with the enhancement of the interparticle interactions. Surprisingly, for the particles heated at higher temperatures, χ_{max} does not

(32) Dormann, J. L.; Fiorani, D.; Tronc, E. *Adv. Chem. Phys.* **1997**, *XC-VIII*, 283.
(33) Fiorani, D.; Testa, A. M.; Tronc, E.; Lucari, F.; , D.; Nogués, M. *J. Magn. Magn. Mater.* **2001**, *1942*, 226–230.
(34) Dormann, J. L.; Bessais, L.; Fiorani, D. *J. Phys.* (*Paris*) **1988**, *C1 21*, 2015.
(35) García-Otero, J.; Parto, M.; Rivas, J.; Bunde, A. *Phys. Rev. Lett.* **2000**, *84*, 167.

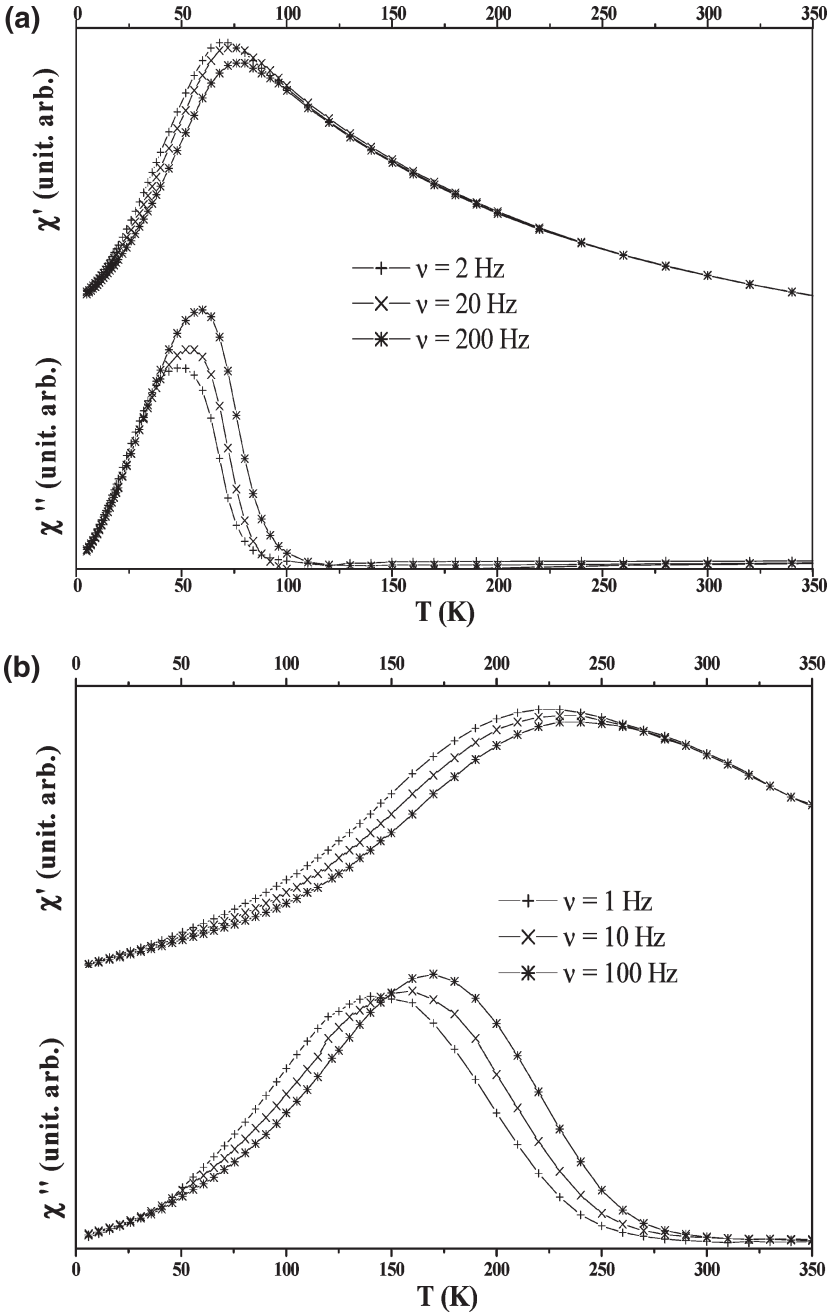

Figure 12. Thermal variation of the ZFC in-phase χ' and out-of-phase χ'' ac suscpetibility of the as-produced $Ni_{0.8}Zn_{0.2}Fe_2O_4$ particles at $\nu = 1$, 10, and 100 Hz (a) and that of those subsequently heated at 400 °C at $\nu = 2$, 20, and 200 Hz (b).

continue to decrease. For instance, χ_{max} decreases from 0.095 $cm^3 \cdot g^{-1}$ for the as-prepared $Ni_{0.8}Zn_{0.2}Fe_2O_4$ particles to 0.036 for the subsequently heated ones at 400 °C particles and then increases up to 0.058 for the subsequently heated ones at 800 °C particles, suggesting a minimum magnetization value for the particles heated at 400 °C. This behavior is also observed when one compares the variation of the saturation magnetization measured at 5 K between the as-produced particles and the subsequently heated ones at different temperatures.

The variation of magnetization with the applied field at 5 K was plotted in Figure 13 for all prepared samples. A hysteresis loop is observed, whatever the Zn content, in agreement with ferrimagnetic behavior. At low field, the loop exhibits a weak coercivity and remanence, typical of soft-ferrimagnetic materials, decreasing slightly with the Zn content. At high field, the magnetization increases almost linearly and saturates at a field as high as 10 kOe for the as-prepared particles and the subsequently heated ones at 800 °C, while it shows a lack of saturation at a field as high as 50 kOe for the ones heated at 400 °C, in fair agreement with the previously evidenced canting effect in these specific samples. This lake of saturation is less important in the samples heated at 600 °C. In all the cases, the saturation magnetization was estimated by extrapolating the curve M vs $1/H$ to zero. The obtained saturation magnetization value, M_{sat}, of as-prepared particles is estimated to be about

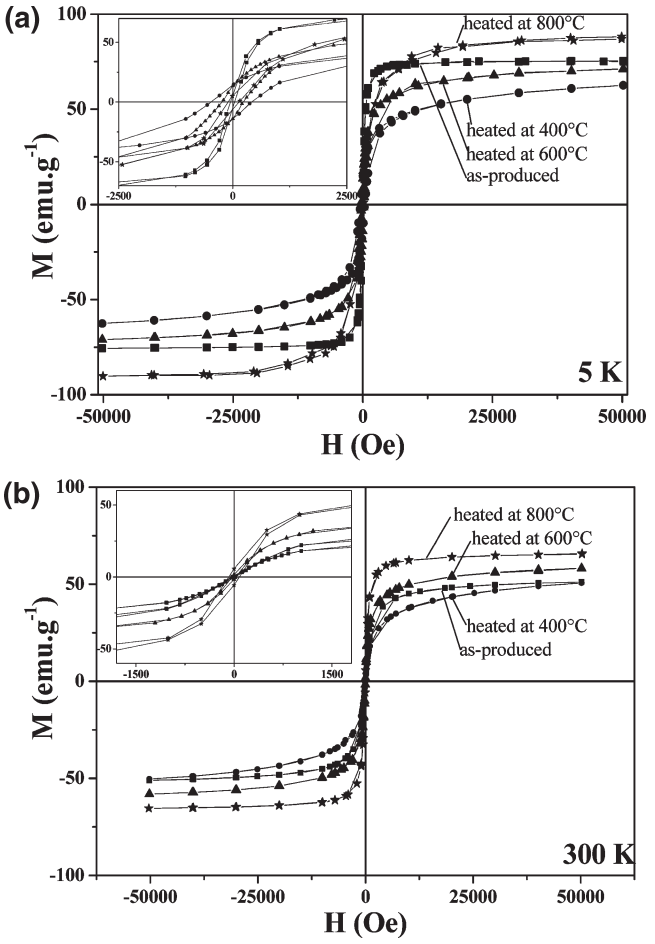

Figure 13. Plot of the 5 (a) and 300 K (b) magnetization as a function of the applied field measured on the as-produced and subsequently heated at 400, 600, and 800 °C $Ni_{0.8}Zn_{0.2}Fe_2O_4$ particles. A zoom of the $H = 0$ region is given in the inset.

85−86% of that of bulk ferrite,[36] while it decreases up to 65−67% of that of bulk for the subsequently heated ones at 400 °C and recovers progressively the bulk value for the heated ones at higher temperature (Table 5). At 800 °C, the measured saturation magnetization at 5 K is equal to that reported for bulk $Ni_{1-x}Zn_xFe_2O_4$ solid solution.

The saturation magnetization measured at 5 K for the as-prepared particles (76 emu·g^{-1}) are significantly higher than those of $Ni_{1-x}Zn_xFe_2O_4$ nanoparticles obtained by other chemical routes[37−39] and very close to that of the bulk (86 emu·g^{-1}). This enhancement could be due to a cation distribution change. Mössbauer and EXAFS studies established the presence of nickel and zinc ions in both tetrahedral and octahedral sites. It could be also due to the exceptional crystalline quality of the particles. HRTEM images show very well-defined particles.

The decrease of the saturation magnetization in the samples heated at 400 °C despite a measured crystal size increase could be explained by the influence of these interparticle interactions. Also, ac-magnetometry measurements have shown that interparticle interactions (mainly dipolar) are particularly important in the particles heated at 400 °C compared to the as-produced ones. But as mentioned previously, whereas the densification process of the powders increases with the heating temperature in the studied sample series, we observe that the saturation magnetization measured at 5 K does not continue to decrease when the heating temperature increases. It exhibits a minimum for the particles heated at 400 °C whatever their zinc content. To the best of our knowledge, only a competition between the crystal size increase and the interparticle interactions improvement when the heating temperature increases can be incriminated to explain this unusual behavior. Such an explanation should be satisfactory if the coercivity exhibits also a decrease of its value when it is measured at 5 K from the as-produced particles to the subsequently heated one at 400 °C. Unfortunately, this is not the case (Figure 14). Surprisingly, the coercivity exhibits a maximum at 400 °C and decreases then progressively when the heating temperature increases up to 800 °C (Table 5).

Discussion

The most interesting result reported in the present study is related to the saturation magnetization and coercivity variation as a function of annealing temperature. Indeed, if the blocking temperature continues to increase when the heating temperature increases, in agreement with the crystal size increase and interparticle interaction enhancement, the saturation magnetization and the coercivity, measured in the blocked state, show a minimum and a maximum, respectively, for the particles heated at 400 °C. Moreover, if one except the case of annealed at 400 °C particles, the measured M_{sat} and H_c values at 5 K are, respectively, very close and quite comparable to that of bulk, even for the as-produced ones.

Usually, the saturation magnetization increases when the annealing temperature increases, because of the grain growth. The lower value of magnetization of nanocrystalline materials as compared to the bulk can be explained by surface effects: a large grain boundary volume present in nanocrystalline films[13,46] and a high atomic surface-to-volume ratio of particles in nanocrystalline powders.[14,40] Other mechanisms are also able to likely affect the magnetization:

(i) First, bulk nickel ferrites can be reduced to form Ni and NiO (more probable under air atmosphere) by heating.[54] NiO is very difficult to characterize by X-ray because it displays diffraction peaks at about the same angles as for spinel phase. In this case,

(36) Smith, S.; Wijn, H. P. J. *Ferrites*; Philips Library: Amsterdam, 1961.
(37) (a) Hwang, C. C.; Tsai, J. S.; Huang, T. H. *Mater. Chem. Phys.* **2005**, *93*, 330. (b) Gubbala, S.; Nathani, H.; Koizol, K.; Misra, R. D. K. *Physica B* **2004**, *348*, 317. (c) Caiser, C.; Stefanescu, M. *J. Phys. D: Appl. Phys.* **2002**, *35*, 3035.
(38) Wu, K. H.; Chang, Y. C.; Chang, T. C.; Chiu, Y. S.; Wu, T. R. *J. Magn. Magn. Mater.* **2004**, *283*, 380.
(39) Ichiyanagi, Y.; Uehashi, T.; Yamada, S. *Phys. Stat. Sol. C* **2004**, *1*, 3485.
(40) (a) Kodama, R. H.; Berkowitz, A. E.; McNiff, E. J., Jr.; Foner, S. *Phys. Rev. Lett.* **1996**, *77*, 394. (b) Martinez, B.; Obradors, X.; Balcells, L.; Rouanet, A.; Monty, C. *Phys. Rev. Lett.* **1998**, *80*, 181. (c) Kodama, R. H.; Berkowitz, A. E. *Phys. Rev. B* **1999**, *59*, 6321.

Table 5. Main Magnetic Characteristics of the As-Produced and Subsequently Heated $Ni_{1-x}Zn_xFe_2O_4$ (x = 0.2 and 0.4) Particles

heating treatment	x	T_B(200 Oe) K	M_{sat}(5 K) emu·g^{-1}	H_c(5 K) Oe	M_{sat}(300 K) emu·g^{-1}	H_c(300 K) Oe
as-	0.2	47	75.9	43	53.0	0
produced	0.4	53	88.9	37	58.0	0
heated at	0.2	179	67.0	408	54.0	0
400 °C	0.4	188	83,5	364	60.5	0
heated at	0.2	> 330	74.4	274	60.7	46
600 °C	0.4	> 330	103.5	238	70.2	31
heated at	0.2	> 330	91.0	123	66.7	80
800 °C	0.4	> 330	113.2	81	76.3	37

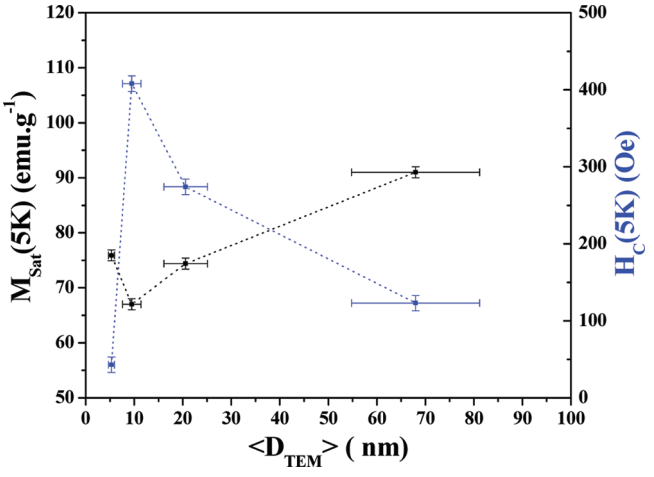

Figure 14. Plot of the 5 K-M_{sat} (left axis) and 5 K-H_c (right axis) as a function of the average TEM measured diameter of the $Ni_{0.8}Zn_{0.2}Fe_2O_4$ particles.

some ferrous ions are created in the octahedral sites of the spinel structure to compensate nickel segregation. Due to their high magnetic moment ($4\,\mu_B$) and their contribution to magnetocrystalline anisotropy (the fundamental spectroscopic term of oxygen octahedrally coordinated Fe^{2+} is $^5T_{2g}$), the reduction could explain the results obtained at 400 °C, namely a decrease of the magnetization (Fe^{2+} cations of $4\,\mu_B$ replace Fe^{3+} ones of $5\,\mu_B$) and an increase of the coercivity. At higher temperature, the spinel ferrite particles are oxidized and the previous effect on M_{sat} and H_c disappears.

(ii) The change in the defect structure is in terms of dislocation and stacking faults on one hand and chemical heterogeneity on the other hand. The density of defects does decrease upon annealing leading to a magnetization increase with the heating temperature increase.

(iii) The cation distribution is strongly dependent on the chemical route used to prepare the nanomaterials, as well as the subsequent annealing conditions. For instance, if a large number of Ni^{2+} cations are on tetrahedral spinel sites and reversely Fe^{3+} ones move to octahedral ones, in the as-prepared nanomaterials, an increase in the magnetic moment should be observed. Heating permits the structure to recover its thermodynamic stable structure, namely to localize Ni^{2+} cations exclusively in the octahedral sites and then to reduce the magnetization.

(iv) The interparticle interactions are improved in the powders obtained after annealing treatment because of the departure of the adsorbed organic matter from the surface of the polyol-made particles, which become close to each other. Strong dipolar interactions favor thus the installation of a collective magnetic glass state leading to a magnetization decrease because of nonhomogeneous and frustrated macro-spin cluster freezing.

Let us consider these different factors one by one. Concerning the chemistry phenomena, nickel segregation (Ni and/or NiO) might occur at 400 °C because of carbon contamination at the surface of the particles. Carbon contamination is very weak, i.e. about 1.5 wt % on the as-produced particles, and decreases down to 0.2 wt % on the subsequently heated particles at 400 °C in air. That means the number of Ni^{2+} cations reduced into Ni (and then oxidized in air into NiO) during the annealing treatment must be very small, corresponding, thus, to a very few amount of formed Fe^{2+} ions into the spinel lattice. Moreover, Mössbauer spectrometry is a very sensitive technique to detect Fe^{2+} species. The limit of detection is usually estimated to be about 1%. The recorded spectra on all studied samples do not evidence at all the presence of such Fe species. We can thus consider that the reduction/oxidation of nickel phenomena in the present nickel−zinc ferrite particle series is negligible and cannot explain the measured magnetic properties.

Concerning the microstructure of the particles, TEM and HRTEM analyses of the heated particles have clearly evidenced that they exhibit a high crystalline quality. XEDS mapping and EFTEM imaging have shown that they are homogeneous without any chemical segregation into each particle or from one particle to another. In the case of the as-produced particles, the obtained magnetic results suggest that they do not exhibit significant structural and microstructural defects. Indeed, first, despite their very reduced size (~5 nm) the thickness of their surface canted layer inferred from in-field Mössbauer analysis[41,42] is very weak: less than 0.2 nm. This thickness is much smaller

(41) Coey, J. M. D. *Phys. Rev. Lett.* **1971**, *27*, 1140.
(42) Tronc, E.; Prené, P.; Jolivet, J. P.; Dormannn, J. L.; Grenèche, J.-M. *Hyperfine Interact.* **1998**, *112*, 97.

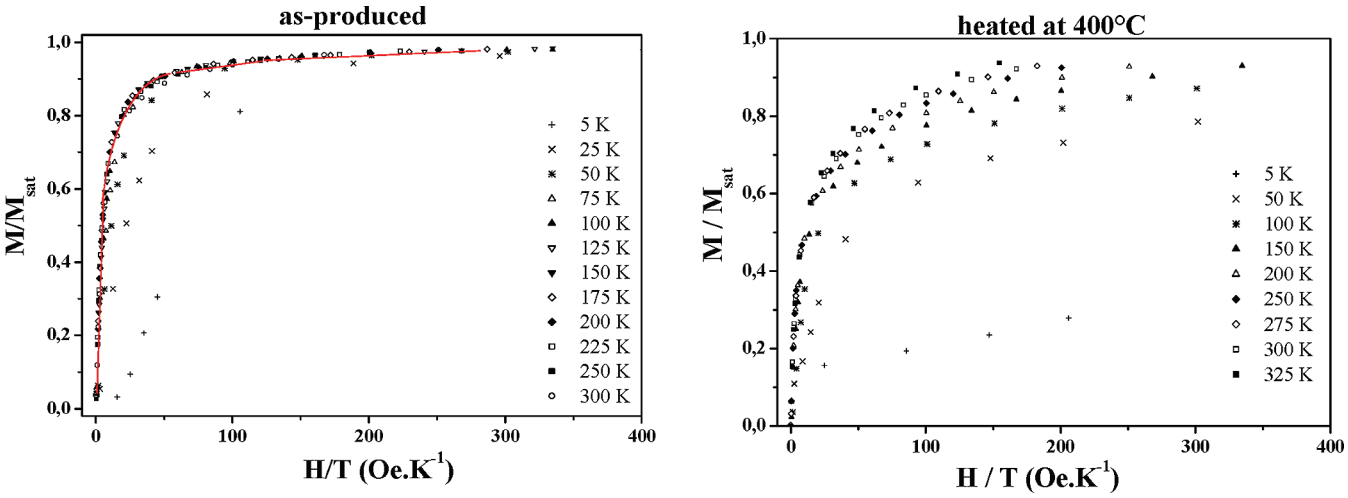

Figure 15. Plot of the M/M_{sat} vs H/T of the as-produced and subsequently heated at 400 °C $Ni_{0.8}Zn_{0.2}Fe_2O_4$ particles. The red continuous line corresponds to the Langevin function fit.

than that usually observed on ferrite nanoparticles: 0.6 nm[42−44] prepared by other chemical routes. Clearly for these particles, the magnetic path break effect due to their finite size is minimal. Second, the variation of the magnetization of these particles as a function of H, when it is measured at low temperature, does not exhibit a significant lack of saturation at high field (Figure 13). The variation of the magnetization as a function of H/T, when it is measured at $T > T_B$, follows a Langevin-type law (Figure 15). The $M(T)/M_{sat}$ vs H/T curves coalesce at $T > T_B$ and are perfectly reproduced using the equation:

$$M(T) = M_{sat}\{\coth(\mu H/kT) - (kT/H)\} + \chi_a H \qquad (3)$$

where μ is the magnetic moment per particle, k is the Boltzmann constant, $M(T)$ is the magnetization of particles for a given temperature T, M_{sat} is the total saturation of the overall particle, M_s is the total saturation of the bulk counterpart, and χ_a is the high-field susceptibility[47] which corresponds to a small correction to the classical Langevin equation[48] due to the finite size of the particles. The magnitude of μ is determined from the equation:

$$\mu = M_s \rho V \qquad (4)$$

where ρ and V are the density and volume of the particle, respectively. Assuming a spherical particle shape with an average diameter $D = 5.4$ nm and a density of $\rho = 5.0\ g\cdot cm^{-3}$ for $Ni_{0.8}Zn_{0.2}Fe_2O_4$, the fit yields $M_s = 81$ emu·g^{-1}, in agreement with the expected value for bulk ferrite. These results show that these polyol-made particles can be considered as almost perfectly magnetically ordered single domain without significant surface and/or core magnetic disorder inducing canting in the magnetic structure nor drastically influenced by strong dipolar interactions. Chemical segregation in such particles is also less probable, since Zn rich Ni−Zn ferrite must exhibit a Yafet−Kittel-like canted magnetic structure: the magnetization vs H/T could not be strictly described using the Langevin law.

The local structure of the particles, in term of cation distribution toward the tetrahedral and octahedral site of the spinel lattice, changes when these are heated. Indeed, the partial transfer of Ni^{2+} from B to A sites leads to an increase of the magnetization according to the collinear ferrimagnetic Néel theory. The reverse transfer of Zn^{2+} from A to B sites leads to its decrease. The simple theoretical expression for the net moment M, for instance, for the as-prepared $Ni_{0.8}Zn_{0.2}Fe_2O_4$ particles, corresponding to the $(Zn_{0.12}Ni_{0.10}Fe_{0.78})[Ni_{0.70}Zn_{0.08}Fe_{1.22}]O_4$ cation distribution, should be addressed as follows:

$$\begin{aligned} M &= M_B - M_A \\ &= [2\times 0.70 + 0\times 0.80 + 5\times 1.22] - (0 \\ &\quad \times 0.12 + 2\times 0.10 + 5\times 0.78) \end{aligned} \qquad (\text{Eq.5})$$

where M_A (square-brackets) and M_B (parentheses) represent the total magnetic moment of the A and B sublattices, respectively. The magnetic moment of Fe^{3+} cations is fixed to 5 μ_B, that of octahedrally and tetrahedrally coordinated Ni^{2+} cations is fixed to 2 μ_B (spin only). Finally, the saturation magnetization is found to be 3.4 μ_B (81.1 emu·g^{-1}) instead of 3.6 μ_B (85.9 emu·g^{-1}) expected for the same ferrite composition with the thermodynamic stable structure where Ni^{2+} and Zn^{2+} cations are exclusively octahedrally and tetrahedrally coordinated, respectively. These two values are very close because the magnetization increase expected by the partial transfer of

(43) Tronc, E.; Ezzir, A.; Cherkaoui, R.; Chanéac, C.; Noguès, M.; Kachkachi, H.; Fiorani, D.; Testa, A. M.; Grenèche, J.-M.; Jolivet, J. P. *J. Magn. Magn. Mater.* **2000**, *221*, 63.
(44) (a) Morrish, A. H.; Haneda, K. *J. Appl. Phys.* **1981**, *52*, 2496. (b) Daou, T. J.; Grenèche, J.-M.; Pourroy, G.; Buathong, S.; Derory, A.; Ulhaq-Bouillet, C.; Donnio, B.; Guillon, D.; Begin-Colin, S. *Chem. Mater.* **2008**, *20*, 5869.
(45) Dormann, J. L.; Fiorani, D.; Cherkaoui, R.; Spinu, L.; Lucari, F.; D'Orazio, F.; Noguès, M.; Tronc, E.; Jolivet, J. P.; Garcia, A. *Nanostruct. Mater.* **1999**, *12*, 757.
(46) Dessai, M.; Dash, J.; Samajdar, I.; Venkataramani, N.; Prasad, S.; Kishan, P.; Kumar, N. *J. Magn. Magn. Mater.* **2001**, *231*, 108.
(47) Dutta, P.; Manivannan, A.; Seehra, M. S.; Shah, N.; Huffman, G. P. *Phys. Rev. B* **2004**, *70*, 174428.
(48) Charles, S. W.; Popplewell, J. *Ferromagnetic Materials*; North Holland Publishing: Amsterdam, 1982.

Ni^{2+} cations from the B sites to the A ones is almost completely compensated by the reverse transfer of Zn^{2+} cations from A sites to B ones. The deviation from the thermodynamic stable structure decreasing in the subsequently heated particles (only 7% of the Ni^{2+} cations are transferred from B to A sites and reversely about 5% of the Zn^{2+} cations are transferred from A to B sites in the $Ni_{1-x}Zn_xFe_2O_4$ particles heated at 400 °C). For a given composition, the saturation magnetization should slightly increase. For instance, when $x = 0.2$, the calculated saturation magnetization of the subsequently heated sample at 400 °C, based on the chemical composition proposed in Table 4, namely $(Zn_{0.18}Ni_{0.02}Fe_{0.84})$-$[Ni_{0.78}Zn_{0.02}Fe_{1.16}]O_4$ and corrected as $(Zn_{0.12}Ni_{0.10}$-$Fe_{0.80})[Ni_{0.70}Zn_{0.08}\ Fe_{1.20}]O_4$ in respect to the stoichiometry, gives a theoretical value of 3.52 μ_B (84.0 emu·g^{-1}) higher than the 3.4 μ_B (81.1 emu·g^{-1}) previously estimated for the as-produced sample. This calculation shows that the magnetization weakly increases by heating. So, one can consider that the magnetization is slightly affected by the cation distribution evolution and consequently the observed cation distribution evolution by heating, in the studied particle series, cannot explain the observed drastic change in the M_{sat} value, particularly from the as-produced particles to the subsequently heated ones at 400 °C.

The interparticle interactions, mainly dipolar ones, usually induce a collective behavior between superparamagnetic particles, decreasing their saturation magnetization and their coercivity measured in their blocked state.[33,45] If one considers the thermal variation of the out-of-phase ac-susceptibility component at different frequencies of the as-prepared particles and that of the subsequently heated one at 400 °C (Figure 12) and its frequency dependency, we can note that the former are consistent with almost weakly interacting superparamagnets, while the later as strongly interacting ones. The high aggregation state of the heated particles compared to the as-prepared ones, should improve the strength of these interactions participating in the reduction of the M_{sat} and H_c values. Paradoxally, data listed in Table 5 allow us to conclude, except for the particles heated at 400 °C, the higher the annealing temperature, the higher the aggregation of particles, the larger the saturation magnetization. The magnetization decreases from the as-prepared particles to the subsequently heated ones at 400 °C, but it increases for the particles heated at higher temperature, exhibiting values very close to that of the bulk. Moreover, these interactions cannot explain at all the so large coercivity values measured on the interacting particles, corresponding to the subsequently heated ones at 400 °C, compared to those of the weakly interacting as-prepared particles. It appears clearly that the magnetic characteristics of our materials completely differ from those described in the literature for nanocrystalline Ni−Zn ferrite powders, and other parameters must be looked for to understand the magnetic features observed here. The coercivity measures the required magnetic field strength for overcoming anisotropy to flip the magnetic moments. In nanoparticles with a single magnetic domain structure, the possible complication from domain wall pinning and movement do not exist. Therefore, the structure- and microstructure-induced magnetic anisotropy can be straightforwardly correlated to coercivity, since dipolar interactions appear to play a minor role. The structure-induced anisotropy, namely the magnetocrystalline anisotropy, is usually defined by the strength of the spin−orbit coupling which is directly related to the local structure of the ferrite, and particularly to the concentration of tetrahedrally coordinated Ni^{2+} cations. The as-prepared particles have about 15% of their Ni^{2+} cations located in the A sites of the spinel lattice. The single-ion anisotropy increase expected for such structural deviation does not lead to a significant increase of the coercivity. The measured H_c values on the as-prepared particles are very weak. In the heated sample, this ratio decreases up to zero, decreasing thus this contribution. The microstructure-induced magnetic anisotropy is usually related to the surface state of the particles and their size and shape. The present particles are almost isotropic in shape, but their size increases when the heating temperature increases, decreasing thus their atomic surface-to-volume ratio and then reducing, theoretically, their surface magnetic disorder induced by the lack of symmetry. Usually, the noncollinearity of magnetic moments in the surface of the particles due to break-up of magnetic exchange paths (surface canting) improves the coercivity (surface anisotropy). An increase in the heating temperature and its corollary particle size increase would be accompanied by a decrease in surface anisotropy and coercivity. This is not the case for the particles heated at 400 °C, because another phenomenon has to be considered: the partial densification of the particles with the creation of grain-boundary-like interfaces between the particles.

It is well-established that the grain boundaries are high intrinsic stress energy regions. For instance, in nanocrystalline films, the presence of such zones was correlated to the increase in H_c.[49,50] The progressive densification of the particles with heating is accompanied by the creation of spin canted interfaces between the particles. The main consequence is a reduction of M_{sat}(5 K) and an increase of H_c(5 K) at the beginning of the process, namely around 400 °C after the departure of the adsorbed organic species. The decrease of the atomic surface-to-volume ratio with particle size increase, when heating at higher temperature, minimizes this phenomenon for the largest particles. To the best of our knowledge, such behavior was never reported on chemically prepared nanoparticles.

(49) Gupta, N.; Verma, A.; Kashyap, S. C.; Dube, D. C. *J. Magn. Magn. Mater.* **2007**, *308*, 137.
(50) Beji, Z.; Smiri, L. S.; Vaulay, M.-J.; Herbst, F.; Ammar, S.; Fiévet, F. Nanocrystalline $Ni_{0.8}Zn_{0.2}Fe_2O_4$ films prepared by spray deposition from polyol-mediated sol: Microstructural and Magnetic Characterization. Thin Solid Films, in press.
(51) (a) O'Neill, H. SI. C.; Navrotsky, A. *Am. Mineral.* **1983**, *68*, l8 1. (b) O'Neill, H. SI. C.; Navrotsky, A. *Am. Mineral.* **l984**, *69*, 733.
(52) Urusov, V. S. *Phys. Chem. Minerals.* **1983**, *9*, 1.
(53) Navrotsky, A.; Kleppa, O. *Inorg. Chem.* **1967**, *6*, 2119.
(54) (a) Elwell, D; Parker, R.; Tinsley, C. J. *Czech. J. Phys.* **2005**, *17*, 382. (b) Irvine, J. T. S.; Huanosta, A.; Valenzuela, R.; West, A. R. *J. Am. Ceram. Soc.* **2005**, *73*, 729.

It is very often masked by the almost poor crystalline quality of the as-prepared particles and by their initial aggregation state.

Conclusion

Nonaggregated, isotropic, and almost monodisperse $Ni_{0.8}Zn_{0.2}Fe_2O_4$ and $Ni_{0.6}Zn_{0.4}Fe_2O_4$ nanoparticles have been successfully prepared by forced hydrolysis in polyol. They exhibit a superparamagnetic behavior at room temperature and a ferrimagnetic one at low temperature. Heating at different temperatures ranged from 400 to 800 °C provides changes of the magnetic properties of these particles. Their blocking temperature increases with their size increase and their aggregation state increase in relation with stronger interparticle interactions. Their saturation magnetization increases when the particle size increases except for the samples corresponding to the heating treatment at 400 °C. A minimum of the saturation magnetization and a maximum of the coercivity are observed at low temperature for these samples. Structural, microstructural, and magnetic investigations, including EXAFS spectroscopy, TEM-HRTEM observations coupled to EFTEM and XEDS analysis, ^{57}Fe Mössbauer spectrometry, and ac- and dc-magnetometry, suggest that the origin of these changes in M_{sat} and H_c value for these samples specifically is related to a partial densification of powders. The progressive aggregation of the particles successfully achieved by heating is accompanied by the creation of spin canted interfaces between the crystallites. The main consequence is a reduction of $M_{sat}(5\ K)$ and an increase of $H_c(5\ K)$ at the beginning of the process, namely around 400 °C after the departure of the adsorbed organic species. The decrease of the atomic surface-to-volume ratio with crystal size increase minimizes this phenomenon for the largest particles obtained by heating at higher temperature.

Acknowledgment. The CMCU France-Tunisia Cooperation Research Program is thanked for financial support. The authors are indebted to Yanling Li (LCIM2, Paris) for access to the SQUID equipment. They also acknowledge the help extended by Dr. Luca Olivi at the ELLETRA synchrotron ring of Trieste.